Optical absorption in asymmetric double quantum wells driven by two intense terahertz fields*

Wu Hong-Wei(吴宏伟)[a] and Mi Xian-Wu(米贤武)[b)c)†]

[a] College of Physical Science and Mechanical Engineering, Jishou University, Jishou 416000, China
[b] Department of Physics and Information Engineering, Huaihua University, Huaihua 418008, China
[c] Key Laboratory of Terahertz Solid-State Technology, Shanghai Institute of Microsystem and Information Technology, Chinese Academy of Sciences, Shanghai 200050, China

(Received 21 July 2012; revised manuscript received 29 August 2012)

Optical absorption is investigated for asymmetric double quantum wells driven by a resonant terahertz field and a varied terahertz field, both polarized along the growth direction. Rich nonlinear dynamics of the replica peak and the Autler–Townes splitting of various dressed states are systematically studied in undoped asymmetric double quantum wells by taking account of multiple factors, such as the frequency of the varied terahertz field and the strength of the resonant terahertz field. Each electron subband splits into two dressed states when the resonant terahertz field is applied in the absence of the varied terahertz field, the optical absorption spectrum shows the first-order Autler–Townes splitting of the electron subbands. When a varied terahertz field is added into the resonant system, the replica peak and the second-order Autler–Townes splitting of the dressed states near the band edge respectively emerge when the varied terahertz field is non-resonant and resonant with these dressed states. When the strength of the resonant terahertz field is increased, the first-order Autler–Townes double peaks and the replica peak in the optical absorption spectrum shift with the shifts of the dressed states. The presented results have potential applications in electro-optical devices.

Keywords: optical absorption, intense terahertz field, Autler–Townes splitting

PACS: 71.35.Cc, 78.20.Jq, 71.70.Ej **DOI:** 10.1088/1674-1056/22/3/037104

1. Introduction

The optical properties of semiconductor quantum wells (QWs) have been reported in recent years.[1–5] It is well known that the interband optical absorption and emission[6–9] in an undoped semiconductor QW can be modified by an external electric field polarized along the growth direction. The application of the external electric field plays an important role in understanding various interesting phenomena in the semiconductor nano-size structure. A direct-current (dc) electric field is applied along the semiconductor QW growth direction, the Franz–Keldysh effect (FKE)[10,11] and the quantum confine Stark effect (QCSE)[12] have been studied in the semiconductor QW. An alternating-current (ac) electric field applied normal to the QW modulates the interband absorption, in particular, the electro-optic modulation by a terahertz (THz) electric field is of great interest. The development of THz field sources in recent years provides unique opportunities to investigate the effects of semiconductor nonlinear optics such as the ac-Stark effect,[13] Rabi flopping,[14–16] and dynamical FKE (DFKE).[17,18] The reason for applying a THz field is the fact that the intersubband transition frequency in the conduction or valence band falls in the THz frequency range. With much effort focused on the theoretical and experimental studies of the optical absorption in the semiconductor QW system driven by an intense THz field, the dependence of the interesting optical absorption features on the intensity, frequency, and phase of the THz field have been explored in detail.[19–24] A replica peak, a sideband peak, and Autler–Townes (A–T) double peaks[25,26] emerge in the optical absorption spectrum for changing the frequency of the intense THz field. With the THz field strength increasing, the DFKE induces a blue-shift of all exciton peaks. However, the ac-Stark shifts depend on whether the THz field is tuned above or below the transition frequency of the intersubband.[27,28] If the frequency of the THz field is tuned below the resonant transition frequency, the two subbands will repel each other; if the frequency of the THz field is tuned above the resonant transition frequency, the two subbands will attract each other by increasing the strength of the THz field. While if the frequency of the THz field equals to the resonant transition frequency, the space of the double peaks of the A-T splitting becomes more pronounced as the intensity of the THz field is increased. Though the optical properties of the semiconductor QW have been studied many times, the semiconductor QW is either driven by an intense THz field or by an intense THz field and a dc electric field.[19,20,22] The optical properties of the semiconductor QW are unclear when two intense THz fields are applied. Furthermore, investigations presented before mostly neglect the variation of the total

*Project supported by the National Natural Science Foundation of China (Grant No. 10647132) and the Hunan Provincial Education Department Funded Project, China (Grant No. 10A100).

†Corresponding author. E-mail: xwmi@yahoo.com.cn

© 2013 Chinese Physical Society and IOP Publishing Ltd

carrier density by using the quasi-equilibrium approximation in the dipole lifetime for the interaction between the external electric field and the matter.[16,22,24] In fact, the carrier concentration is sensitive when the external optical field interacts with the semiconductor quantum well system. Thus, in this paper, we calculate the optical absorption of asymmetric double quantum wells in the presence of a resonant THz field and a varied THz field by establishing self-consistent density matrix equations. Replica peaks of the dressed states emerge for the frequency of the varied THz field which is non-resonant with the transition frequency between these dressed states of the electron subbands when fixing the resonant THz field. The second-order A–T splitting (the A–T splitting induced by a resonant THz field only is called the first order A–T splitting, and that induced by a varied THz field in the presence of another resonant THz field is called the second-order A–T splitting in this paper) occurs when the varied THz field is tuned to the resonant transition frequency. When the varied THz field is fixed, the left and the right main peaks of the first A–T splitting of the first electron subband respectively red and blue shift for the increasing strength of the resonant THz field. Simultaneously, the replica peak of the dressed states shifts with the shift of the dressed states. The presented results interpret the optical absorption features of semiconductor asymmetric double quantum wells (ADQWs) driven by two THz fields and play an important role for understanding the optical-electro properties of the semiconductor quantum well.

2. Theoretical framework

The QW structure studied here has asymmetric coupled quantum wells, and which contains two different-width GaAs QWs coupled through a thin middle AlGaAs barrier. The electron and hole states of the semiconductor QW are calculated by using the $\boldsymbol{k}\cdot\boldsymbol{p}$ perturbation theory. We can write the single particle Hamiltonian as

$$H(r) = -\frac{\hbar(\partial_x^2+\partial_y^2)}{2m_{\parallel}^*(x,y)} - \frac{\hbar\partial_z^2}{2m_{\perp}^*(z)} + V(z),$$

where $m_{\parallel}^*(x,y)$ is the electron (hole) effective mass for the motion in the QW layer plane, $m_{\perp}^*(z)$ is the electron (hole) effective mass for the motion in the z direction of the QW, and $V(z)$ is the potential energy, which is determined by the band offsets of the conduction or valence band in the QW region. We can obtain the electron envelope function $\left|\varphi_{nk}^{\mathrm{e}}(r)\right\rangle$ and eigenenergy $\varepsilon_n^{\mathrm{e}}$ (the hole envelope function $\left|\psi_{lk}^{\mathrm{h}}(r)\right\rangle$ and eigenenergy $\varepsilon_l^{\mathrm{h}}$) by solving a set of secular equations which come from the eigenequation by imposing the periodic boundary condition, where n and l are the indexes of conduction and valence subbands, respectively.

In this paper, we consider a three-level system (TLS), which is constructed with the first and the second electron subbands and the first hole subband of the ADQWs. The optical absorption of the TLS is considered for the semiconductor ADQWs driven by intense electric fields along the growth direction and a weak near-infrared (NIR) probe beam. The growth direction electric fields are a resonant terahertz field and a varied terahertz field, which can be expressed as $F(t) = F_{\mathrm{THz}}^{\mathrm{res}}\cos(2\pi\nu_{\mathrm{THz}}^{\mathrm{res}}t) + F_{\mathrm{THz}}^{\mathrm{var}}\cos(2\pi\nu_{\mathrm{THz}}^{\mathrm{var}}t)$, where $F_{\mathrm{THz}}^{\mathrm{res}}$ and $\nu_{\mathrm{THz}}^{\mathrm{res}}$ are the intensity and the frequency of the resonant THz field, $F_{\mathrm{THz}}^{\mathrm{var}}$ and $\nu_{\mathrm{THz}}^{\mathrm{var}}$ are the intensity and the frequency of the varied THz field, respectively. The NIR probe beam is given by $E_{\mathrm{opt}}(t) = E_0\exp(-t^2/\tau^2 - \mathrm{i}\omega_{\mathrm{c}}t) + \mathrm{c.c.}$, where $E_0 = 14$ kV/cm, the duration time is $\tau = 15$ fs. In order to investigate the optical absorption dynamics of the band edge, the central frequency of the Gaussian optical pulses is tuned to the band gap frequency. In the presence of two THz fields and an NIR probe beam, the full Hamiltonian of the TLS is given by

$$H = H_0 + H_{\mathrm{C}} + H_{\mathrm{I}}^{\mathrm{opt}} + H_{\mathrm{I}}^{\mathrm{THz}}. \tag{1}$$

The first term H_0 contains the single particle energies of electrons and holes, and can be written for the TLS as

$$H_0 = \sum_{n=1k,2k}\left(\varepsilon_{nk}^{\mathrm{e}}\alpha_{nk}^{+}\alpha_{nk} + \varepsilon_{1k}^{\mathrm{h}}\beta_{1-k}^{+}\beta_{1-k}\right), \tag{2}$$

where $\varepsilon_{n=1k}^{\mathrm{e}}$, $\varepsilon_{n=2k}^{\mathrm{e}}$, and $\varepsilon_{1k}^{\mathrm{h}}$ correspond to the first and the second electron subband energy levels and the first hole subband energy level of the TLS, respectively, α_{nk}^{+} and α_{nk} are the creation and annihilation operators for the electron in the n-th subband of the conduction band, respectively, and β_{1k}^{+} and β_{1k} are the creation and annihilation operators for the hole in the first subband of the valence band, respectively. The second term in Eq. (1) describes the electron–hole Coulomb interaction. When only considering the TLS in the ADQWs, it can be expressed as

$$H_{\mathrm{C}} = \sum_{kk'q\neq 0}^{n,n'=1,2}\left(\alpha_{nk+q}^{+}\beta_{1k'-q}^{+}\beta_{1k'}\alpha_{n'k}\right)V_{nn'11}(q), \tag{3}$$

where $n,n' = 1,2$, $V_{2111}(q)$ and $V_{1211}(q)$ are the Coulomb interaction matrix elements between excitons χ_{e1h1} (an electron and a hole locate at the first electron subband and the first hole subband, respectively) and χ_{e2h1} (an electron and a hole locate at the second electron subband and the first hole subband, respectively). The two matrix elements have the relationship $V_{2111}(q) = V_{1211}^{*}(q)$. In the semiconductor ADQWs, the TLS is driven by two continue wave-THz fields and a continue wave-NIR probe beam. However, the resonant and the varied THz fields couple to the two electron subbands and the interband optical absorption occurs in the presence of the continue wave-NIR beam. Therefore, the interaction term is contained in the third and the fourth terms of the Hamiltonian. The third term describes the dipole interaction between the NIR beam and the TLS, inducing the interband polarization. The fourth term describes the interaction between the growth

direction electric field and the subbands, inducing intraband transition in the conduction band of the TLS. Thus, the third and the fourth terms can be written as

$$H_{\mathrm{I}}^{\mathrm{opt}} = \sum_{n=1k,2k} \left(u_{n1k}\alpha_{nk}^{+}\beta_{1-k}^{+} + u_{n1k}^{*}\beta_{1-k}\alpha_{nk}\right)E_{\mathrm{opt}}(t), \quad (4)$$

$$H_{\mathrm{I}}^{\mathrm{THz}} = F(t)\sum_{k}\left(\mu_{12}\alpha_{1k}^{+}\alpha_{2k} + \mu_{21}\alpha_{2k}^{+}\alpha_{1k}\right), \quad (5)$$

where u_{n1k} is the interband dipole matrix element for the transition between the electron state and the hole state in Eq. (4). If $n=1$, $u_{11k} = u_0\left\langle\varphi_{1k}^{\mathrm{e}}(r)|\psi_{1k}^{\mathrm{h}}(r)\right\rangle$, if $n=2$, $u_{21k} = u_0\left\langle\varphi_{2k}^{\mathrm{e}}(r)|\psi_{1k}^{\mathrm{h}}(r)\right\rangle$, where u_0 is the optical dipole matrix element, for GaAs QW, $u_0 = 4.9$ eÅ. The μ_{12} is the intersubband dipole matrix element for the transition from the first electron subband to the second electron subband, $\mu_{12} = \mu_{21}^{*} = -\left\langle\varphi_{1k}^{\mathrm{e}}(r)\right|ez\left|\varphi_{2k}^{\mathrm{e}}(r)\right\rangle$, where e is the free electron change.

Optical absorption coefficient $\sigma(\omega)$ is related to the macroscopic interband polarization $P(z,t)$ when the NIR probe interacts with the semiconductor TLS driven by the resonant and the varied THz fields. However, the macroscopic polarization of the system is connected to the microscopic interband polarization p_{1nk}, which is define as $p_{1nk} = \beta_{1-k}\alpha_{nk}$, $n = 1,2$ for the TLS. The relation between the macroscopic n and the microscopic polarizations is

$$P(t) = \sum_{n=1k,2k} u_{1nk}^{*}p_{1nk} + \mathrm{c.c.} \quad (6)$$

Considering the variation of the carrier concentration, we can obtain the self-consistent motion equtions of the microscopic polarization and the carrier concentration by using the Heisenberg equation as follows:

$$\begin{aligned}\hbar\frac{\partial f_{nn'k}^{\mathrm{e}}}{\partial t} = \sum_{nn'=1,2}\big\{ & -\mathrm{i}[\varepsilon_{nk}^{\mathrm{e}} - (1-\delta_{nn'})\varepsilon_{n'}^{\mathrm{e}}]f_{nn'k}^{\mathrm{e}} \\ & + \mathrm{i}F(t)(\mu_{nn'}f_{nn'k}^{\mathrm{e}} + \mu_{n'n}f_{n'nk}^{\mathrm{e}}) \\ & + \mathrm{i}E_{\mathrm{opt}}(t)(u_{n'1k}p_{1nk}^{*} - u_{n1k}^{*}p_{1n'k}) \\ & - \mathrm{i}(U_{n1k}p_{1n'k}^{*} - U_{n'1k}^{*}p_{1nk}) \\ & - \gamma_{\mathrm{intra}}(1-\delta_{nn'})f_{nn'k}^{\mathrm{e}}\big\}, \end{aligned} \quad (7)$$

$$\begin{aligned}\hbar\frac{\partial f_{11-k}^{\mathrm{h}}}{\partial t} = \sum_{n=1,2}\big[& -\mathrm{i}\varepsilon_{1-k}^{\mathrm{h}}f_{11-k}^{\mathrm{h}} \\ & + \mathrm{i}E_{\mathrm{opt}}(t)(u_{1nk}p_{1nk}^{*} - u_{1nk}^{*}p_{1nk}) \\ & - \mathrm{i}(U_{n1k}p_{1nk}^{*} - U_{n1k}^{*}p_{1nk})\big], \end{aligned} \quad (8)$$

$$\begin{aligned}\hbar\frac{\partial p_{1nk}}{\partial t} = \sum_{nn'=1,2}\big[& -\mathrm{i}(\varepsilon_{nk}^{\mathrm{e}} + \varepsilon_{1-k}^{\mathrm{h}} - \hbar\omega_{\mathrm{g}})p_{1nk} \\ & + \mathrm{i}E_{\mathrm{opt}}(t)u_{n1k}(1 - f_{nn'k}^{\mathrm{e}} - f_{11-k}^{\mathrm{h}}) + \mathrm{i}F(t)\mu_{nn'}p_{1nk} \\ & - \mathrm{i}U_{n'1k}(\delta_{nn'} - f_{nn'k}^{\mathrm{e}} - \delta_{nn'}f_{11-k}^{\mathrm{h}}) \\ & - \gamma_{\mathrm{inter}}p_{1nk}\big], \end{aligned} \quad (9)$$

where $f_{nn'k}^{\mathrm{e}}$ is the electron concentration of the n-th electron subband when $n = n'$ and is the intersubband polarization when $n \neq n'$, and f_{11-k}^{h} denotes the hole concentration of the first hole subband. In the above terms, the well-known Hartree–Fock approximation is applied. The Coulomb interaction matrix of electron–hole is $U_{n1k} = -\sum_{n'q\neq 0} V_{nn'11}(q)p_{1n'k+q}$. The last terms of Eqs. (7) and (9) are the dephasing terms from higher-order correlations in the dephasing time approximation. The higher-order correlations (collision terms) mainly describe the carrier–carrier and the carrier–phonon scatterings. The γ_{intra} and γ_{inter} are the intersubband and the interband dephasing rates, respectively. The linear optical absorption spectrum can be calculated from the interband macroscopic polarization and expressed as

$$\sigma(\omega) = \frac{4\pi\omega_{\mathrm{c}}}{c\sqrt{\varepsilon_{\mathrm{b}}}}\cdot\frac{\mathrm{Im}[P(\omega)E_{\mathrm{opt}}^{*}(\omega)]}{|E_{\mathrm{opt}}(\omega)|^2}, \quad (10)$$

where c is the speed of light in vacuum, the background dielectric constant is $\varepsilon_{\mathrm{b}} = 12.4$, $P(\omega)$ and $E_{\mathrm{opt}}(\omega)$ are the Fourier transforms of the polarization function $P(t)$ and the NIR pulse $E_{\mathrm{opt}}(t)$, respectively.

3. Numerical results and discussion

As mentioned in the above, the optical absorption coefficient is proportional to the imaginary part of the first-order susceptibility. In this paper, we consider a semiconductor ADQW structure, which consists of undoped 90 Å and 70 Å GaAs wells separated by a 30 Å $Al_{0.3}Ga_{0.7}As$ middle barrier. The two wells and the middle thin barrier are embedded in two outer $Al_{0.3}Ga_{0.7}As$ barriers. The material parameters[22] of the GaAs well $m_{\mathrm{e}\|}^{*} = m_{\mathrm{e}\perp}^{*} = 0.067m_0$, $m_{\mathrm{h}\|}^{*} = 0.109m_0$, $m_{\mathrm{h}\perp}^{*} = 0.34m_0$ (m_0 is the free-electron mass), and $E_{\mathrm{g}} = 1.424$ eV are applied at low temperature. The material parameters of the $Al_{0.3}Ga_{0.7}As$ barrier $m_{\mathrm{e}\|}^{*} = 0.092m_0$, $m_{\mathrm{e}\perp}^{*} = 0.075m_0$, $m_{\mathrm{h}\|}^{*} = 0.145m_0$, $m_{\mathrm{h}\perp}^{*} = 0.401m_0$, and $E_{\mathrm{g}} = 1.937$ eV are used. The temporal pulse of NIR is 20 fs. The temperature is set at $T = 77$ K. The intersubband and the interband dephasing rates are set to $\gamma_{\mathrm{intra}} = 0.01$ meV and $\gamma_{\mathrm{inter}} = 0.1$ meV, respectively.

Figure 1 is a schematic diagram of the energy levels of the TLS driven by a resonant THz field and a varied THz field. Both the first and the second electron subbands are split into two dressed states (the lower and the upper dressed states) when the resonant THz field couples with the two electron subbands in the absence of the varied THz field. When the varied THz field is applied to the resonant system along the growth direction, these dressed states are tuned by the varied THz field. The NIR probe beam induces the transition between the first hole subband $|\psi_{1k}^{\mathrm{h}}(\boldsymbol{r})\rangle$ and these dressed states $|\varphi_{1k}^{\mathrm{e}}(\boldsymbol{r})\rangle^{\mathrm{lower}}$, $|\varphi_{1k}^{\mathrm{e}}(\boldsymbol{r})\rangle^{\mathrm{upper}}$, $|\varphi_{2k}^{\mathrm{e}}(\boldsymbol{r})\rangle^{\mathrm{lower}}$, $|\varphi_{2k}^{\mathrm{e}}(\boldsymbol{r})\rangle^{\mathrm{upper}}$ when the resonant and the varied THz fields are applied simultaneously. We mainly consider the optical absorption properties of the dressed states near the band edge (i.e, $|\varphi_{1k}^{\mathrm{e}}(\boldsymbol{r})\rangle^{\mathrm{lower}}$ and $|\varphi_{1k}^{\mathrm{e}}(\boldsymbol{r})\rangle^{\mathrm{upper}}$) in the following part.

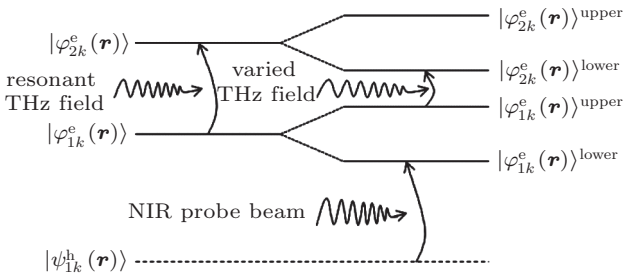


Fig. 1. Schematic diagram of the energy levels of TLS driven by a resonant THz field and a varied THz field. The resonant THz field induces the A–T splitting of the first and the second electron subbands, each electron subband splits into an upper dressed state and a lower dressed state. The varied THz field induces the transition between these dressed states. The interband transition from the first hole subband to the dressed state of the electron subband is induced by the NIR probe beam. Here $|\varphi^{e}_{1k}(r)\rangle^{lower}$ and $|\varphi^{e}_{1k}(r)\rangle^{upper}$ are the dressed states of the first electron subband induced by the resonant THz field, $|\varphi^{e}_{2k}(r)\rangle^{lower}$ and $|\varphi^{e}_{2k}(r)\rangle^{upper}$ are the dressed states of the second electron subband.

Figure 2 shows the optical absorption spectra of the TLS for the semiconductor ADQWs driven by a varied THz field with the frequency in the range from $\nu^{var}_{THz} = 1.8$ THz to $\nu^{var}_{THz} = 3.0$ THz and the strength $F^{var}_{THz} = 15$ kV/cm in the presence of a resonant THz field $\nu^{res}_{THz} = 2.4$ THz, $F^{res}_{THz} = 15$ kV/cm. The first-order A–T splitting occurs when the resonant THz field is applied in the absence of the varied THz field (i.e., $\nu^{var}_{THz} = 0$ THz, $F^{var}_{THz} = 0$ kV/cm), as shown in Fig. 2. The mechanism behind the first-order A–T splitting is that each electron subband is split into two dressed states when the resonant THz field is applied. However, the first-order A–T splitting of the first electron subband becomes obvious when adding the varied THz field. When the frequency of the varied THz field is increased to $\nu^{var}_{THz} = 1.8$ THz, there are two replica peaks in the optical absorption spectrum locating at -7 meV, 3 meV, respectively. The left one is the replica peak of the upper dressed state of the first electron subband because the frequency of the varied THz field is close to the transition frequency between the two dressed states of the first electron subband. Because the transition frequency between states $|\varphi^{e}_{2k}(r)\rangle^{lower}$ and $|\varphi^{e}_{1k}(r)\rangle^{upper}$ is close to $\nu^{var}_{THz} = 1.8$ THz, the right one contains two parts. One is the replica peak of the lower dressed state of the first electron subband, and the other is the replica peak of the lower dressed state of the second electron subband. The dip of the A–T splitting becomes deeper and the separation between the two peaks becomes more pronounced compared with those in the case without the varied THz field. When tuning the frequency of the varied THz field to $\nu^{var}_{THz} = 2.0$ THz, the replica peaks disappear, the transition frequency between states $|\varphi^{e}_{2k}(r)\rangle^{lower}$ and $|\varphi^{e}_{1k}(r)\rangle^{upper}$ is resonant with the THz frequency, the right main peak of the first A–T splitting becomes broad instead of emerging the second-order A–T splitting because the coupling between the two dressed states is too weak to induce the splitting effect. Figure 2(d) shows that the replica peak of state $|\varphi^{e}_{2k}(r)\rangle^{lower}$ emerges at -2 meV when the varied THz frequency is tuned to $\nu^{var}_{THz} = 2.2$ THz. The interaction of the near-resonance THz field is stronger when the detuning between the THz frequency and the intersubband transition frequency is large. Thus, the dynamics of the optical absorption are mainly determined by the near-resonance THz field. When the varied THz frequency is increased to $\nu^{var}_{THz} = 2.4$ THz, the absorption spectrum shows an obvious A–T splitting. In fact, the A–T splitting is similar to that in the case with the resonant THz field $F^{res}_{THz} = 30$ kV/cm, $\nu^{res}_{THz} = 2.4$ THz in absence of the varied THz field. Increasing the varied THz frequency to $\nu^{var}_{THz} = 2.6$ THz, the replica peak of the dressed state $|\varphi^{e}_{2k}(r)\rangle^{upper}$ emerges at -2.3 meV because the THz frequency is close to the transition frequency between the lower dressed state of the first electron subband and the upper dressed state of the second electron subband. In Fig. 2(f), we can find that the left main peak of the first-order A–T splitting becomes weak in magnitude and broad in width, and the strength of the right one becomes strong. The left main peak is split into two symmetric small peaks when the varied THz frequency is tuned to the resonant frequency $\nu^{var}_{THz} = 2.8$ THz between dressed states $|\varphi^{e}_{1k}(r)\rangle^{lower}$ and $|\varphi^{e}_{2k}(r)\rangle^{upper}$. The two symmetric small peaks of the second-order A–T splitting translate into a replica peak and the left main peak for the varied THz frequency is larger than the transition frequency when increasing the varied THz frequency. If the THz frequency is continuely increased, the replica peak moves to the left side until it disappears, and the left main peak recovers.

We now proceed to explore the dependence of the optical absorption on the strength of the resonant THz field when the varied THz field is fixed at the strength $F^{var}_{THz} = 15$ kV/cm and the frequencies $\nu^{var}_{THz} = 2.2$ THz, $\nu^{var}_{THz} = 2.4$ THz, $\nu^{var}_{THz} = 2.6$ THz, $\nu^{var}_{THz} = 2.9$ THz.

Figure 3 shows the dependence of the optical absorption spectrum on the resonant THz strength when the varied THz field is fixed at $\nu^{var}_{THz} = 2.2$ THz, $F^{var}_{THz} = 15$ kV/cm. By increasing the strength of the resonant THz field, the separation between the two main peaks of the first-order A–T splitting is increased. Then, the left main peak red shifts and the right one blue shifts. The replica peak is red shifted with the red shift of the dressed state $|\varphi^{e}_{2k}(r)\rangle^{lower}$ for the increasing resonant THz strength. Simultaneously, the three peaks decrease in magnitude, as shown in Fig. 3. Particularly, the replica peak translates into a footstep when the strength is increased to $F^{res}_{THz} = 22$ kV/cm corresponding to the solid line in Fig. 3.

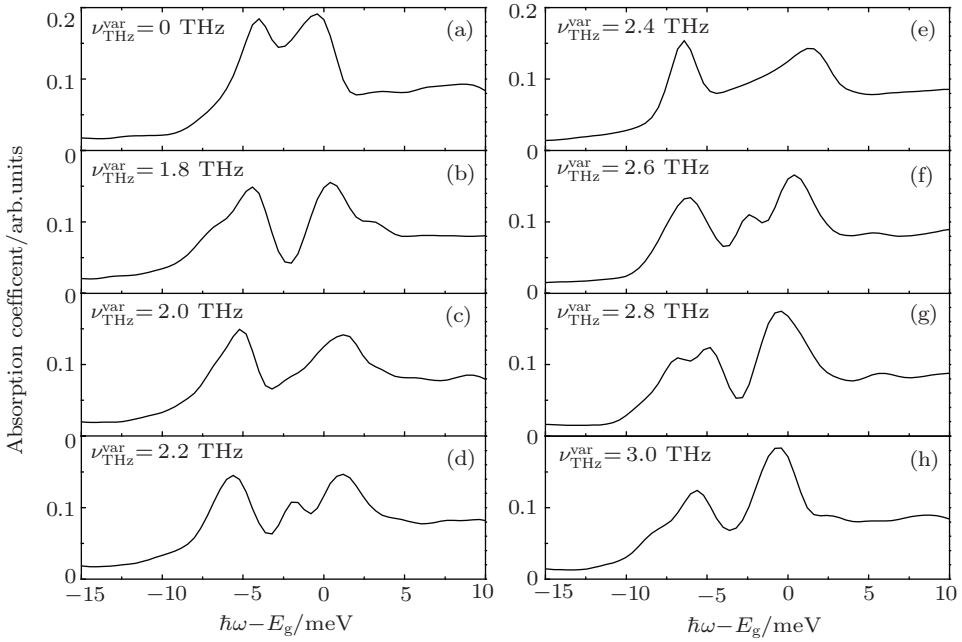


Fig. 2. Optical absorption spectra of the TLS in the presence of the resonant THz field with different frequency varied THz fields. The frequency and the strength of the resonant THz field are $\nu_{\rm THz}^{\rm res} = 2.4$ THz and $F_{\rm THz}^{\rm res} = 15$ kV/cm, respectively. The strength of the varied THz field is $F_{\rm THz}^{\rm var} = 15$ kV/cm, the frequency is (b) $\nu_{\rm THz}^{\rm var} = 1.8$ THz, (c) $\nu_{\rm THz}^{\rm var} = 2.0$ THz, (d) $\nu_{\rm THz}^{\rm var} = 2.2$ THz, (e) $\nu_{\rm THz}^{\rm var} = 2.4$ THz, (f) $\nu_{\rm THz}^{\rm var} = 2.6$ THz, (g) $\nu_{\rm THz}^{\rm var} = 2.8$ THz, (h) $\nu_{\rm THz}^{\rm var} = 3.0$ THz. Panel (a) shows the optical absorption in the absence of the varied THz field.

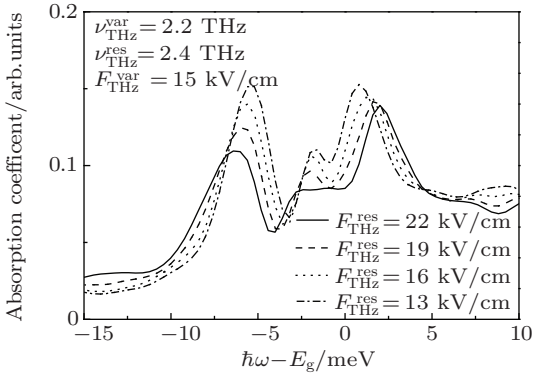


Fig. 3. Absorption spectra for different resonant THz strengths in the presence of the varied THz field $\nu_{\rm THz}^{\rm var} = 2.2$ THz, $F_{\rm THz}^{\rm var} = 15$ kV/cm. The frequency of the resonant THz field is 2.4 THz.

Figure 4 shows the dependence of the optical absorption spectrum on the resonant THz strength when the varied THz field is fixed at $\nu_{\rm THz}^{\rm var} = 2.4$ THz, $F_{\rm THz}^{\rm var} = 15$ kV/cm. The A–T double peaks emerge in the absorption spectra, and the left main peak is dominant over the right one in magnitude when the strength of the resonant THz field is $F_{\rm THz}^{\rm res} = 13$ kV/cm. When the strength is $F_{\rm THz}^{\rm res} = 19$ kV/cm, the two peaks are approximately equal in height, the width of the right main peak is larger than that of the left one. The separation between the two peaks becomes more pronounced with the increase of the resonant THz strength. The phenomenon of peak-shift is the reason why the coupling constant of the resonant THz field increases and the two dressed states shift. When the intensity of the resonant THz field exceeds $F_{\rm THz}^{\rm res} = 19$ kV/cm, the right main peak is dominant over the left one in magnitude, the separation between the two main peaks of the first order A–T splitting is further expanded.

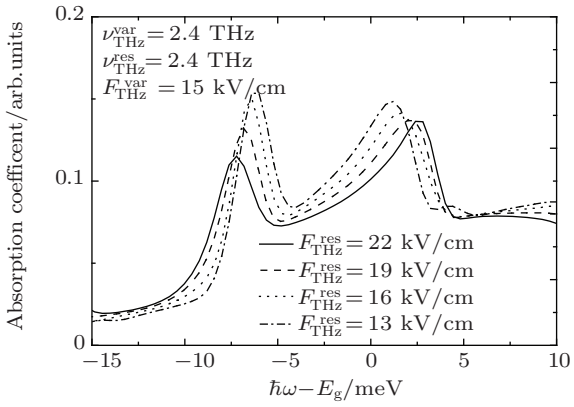


Fig. 4. Absorption spectra for different resonant THz strengths in the presence of the varied THz field $\nu_{\rm THz}^{\rm var} = 2.4$ THz, $F_{\rm THz}^{\rm var} = 15$ kV/cm. The frequency of the resonant THz field is 2.4 THz.

Figure 5 shows the dependence of the optical absorption of the TLS on the resonant THz strength when the varied THz field is fixed at $\nu_{\rm THz}^{\rm var} = 2.6$ THz, $F_{\rm THz}^{\rm var} = 15$ kV/cm. The optical absorption spectrum is similar to the absorption spectra in Fig. 3. The replica peak blue shifts with the blue shift of the upper dressed state of the second electron subband. The decreases of the three peaks in magnitude are small comparing with the case in Fig. 3. Particularly, the replica peak becomes weak in magnitude and broad in width rather than a footstep.

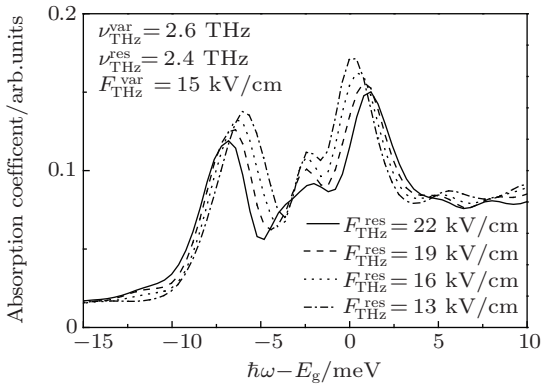


Fig. 5. Absorption spectra for different resonant THz strengths in the presence of the varied THz field $\nu_{\rm THz}^{\rm var}=2.6$ THz, $F_{\rm THz}^{\rm var}=15$ kV/cm. The frequency of the resonant THz field is 2.4 THz.

When the varied THz field is fixed at $\nu_{\rm THz}^{\rm var}=2.9$ THz, $F_{\rm THz}^{\rm var}=15$ kV/cm, the optical absorption spectra for different resonant THz strengths are shown in Fig. 6. The replica peak of the upper dressed state of the second electron subband locates at -6 meV when the strength of the resonant THz field is $F_{\rm THz}^{\rm res}=13$ kV/cm. However, the replica peak disappears and the left main peak is split into two small peaks of the second-order A–T splitting when the strength is $F_{\rm THz}^{\rm res}=16$ kV/cm. If we continue to increase the strength of the resonant THz field, the replica peak emerges again and locates at the right side of the left main peak because the transition frequency between dressed states $|\varphi_{2k}^{\rm e}(\boldsymbol{r})\rangle^{\rm upper}$ and $|\varphi_{1k}^{\rm e}(\boldsymbol{r})\rangle^{\rm lower}$ is increased for the increasing resonant THz strength. The left main peak recovers and red shifts when the strength is increased to $F_{\rm THz}^{\rm res}=22$ kV/cm. The right main peak blue shifts and decreases in magnitude for the increasing strength of the resonant THz field in the whole process.

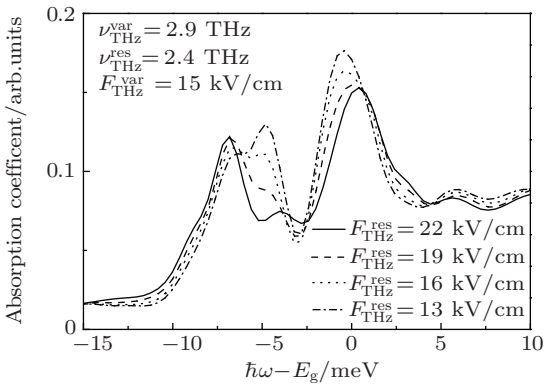


Fig. 6. Absorption spectra for different resonant THz strengths in the presence of the varied THz field $\nu_{\rm THz}^{\rm var}=2.9$ THz, $F_{\rm THz}^{\rm var}=15$ kV/cm. The frequency of the resonant THz field is 2.4 THz.

4. Conclusion

We have presented a detailed study on the absorption spectra of the TLS in semiconductor ADQWs in the presence of a resonant THz field and a varied THz field. Two main peaks of the first-order A–T splitting emerge in the optical absorption spectrum when the resonant THz field is applied in the absence of the varied THz field. However, when the varied THz field is added to the TLS driven by the resonant THz field, the replica peak and the second-order A–T splitting of the dressed states respectively appear when the varied THz frequency is non-resonant and resonant with the transition frequency between the two dressed states. For the dependence of the optical absorption spectrum on the strength of the resonant THz field, the red shift of the left main peak and the blue shift of the right main peak are found for the increasing resonant THz intensity. The replica peak of the dressed state of the electron subband shifts with the shift of the dressed state. The two intense THz fields induced optical absorption, which may be of great use in optical modulator devices operating at the varied THz frequency. Meanwhile, the varied THz field that induced second-order A–T splitting has many potential applications in electric-optical switching.

References

[1] Cao J C and Lei X L 2003 *Phys. Rev. B* **67** 085309
[2] Baur M, Filipp S, Bianchetti R, Fink J M, Goppl M, Steffen L, Leek P J, Blais A and Wallraff A 2009 *Phys. Rev. Lett.* **102** 243602
[3] Sillanpää M A, Li J, Cicak K, Altomare F, Park J I, Simmonds R W, Paraoanu G S and Hakonen P J 2009 *Phys. Rev. Lett.* **103** 193601
[4] Zhang T Y, Zhao W, Liu X M and Zhang C 2007 *Appl. Phys. Lett.* **91** 041909
[5] Duc H T, Meier T and Koch S W 2005 *Phys. Rev. Lett.* **95** 086606
[6] Lei X L, Wang D W, Liang S X and Wu Z X 2012 *Acta Phys. Sin.* **61** 057803 (in Chinese)
[7] Ma X F, Zhou C Y and Wang Y Z 2011 *Acta Phys. Sin.* **60** 068102 (in Chinese)
[8] Li X L, Yang B Z, Yang L J and Zhang L S 2010 *Acta Phys. Sin.* **59** 7008
[9] Liu Z B, Liang Y, Jia K N and Fan X J 2012 *Chin. Phys. B* **21** 024206
[10] Franz W Z 1958 *Naturforsch* **13a** 484
[11] Keldysh L V 1958 *Sov. Phys. JETP* **6** 763
[12] Miller D A B, Chemla D S, Damen T C, Gossard A C, Wiegmann W, Wood T H and Burrus C A 1984 *Phys. Rev. Lett.* **53** 2173
[13] Dynes J F, Frogley M D, Beck M, Faist J and Phillips C C 2005 *Phys. Rev. Lett.* **94** 157403
[14] Luo C W, Reimann K, Woerner M, Elsaesser T, Hey R and Ploog K H 2004 *Phys. Rev. Lett.* **92** 047402
[15] Cole B E, Williams J B, King B T, Sherwin M S and Stanley C R 2001 *Nature* **410** 60
[16] Leinß S, Kampfrath T, Volkmann K V, Wolf M, Steiner J T, Kira M, Koch S W, Leitenstorfer A and Huber R 2008 *Phys. Rev. Lett.* **101** 246401
[17] Srivastava A, Srivastava R, Wang J and Kono J 2004 *Phys. Rev. Lett.* **93** 157401
[18] Chin A H, Bakker J M and Kono J 2000 *Phys. Rev. Lett.* **85** 3293
[19] Maslov A V and Citrin D S 2000 *Phys. Rev. B* **62** 16686
[20] Maslov A V and Citrin D S 2001 *Phys. Rev. B* **64** 155309
[21] Autler S H and Townes C H 1955 *Phys. Rev.* **100** 703
[22] Mi X W, Cao J C and Zhang C 2004 *J. Appl. Phys.* **95** 1191
[23] Wagner M, Schneider H, Stehr D, Winnerl S, Andrews A M, Schartner S, Strasser G and Helm M 2010 *Phys. Rev. Lett.* **105** 167401
[24] Zhang J Z and Allsopp D 2009 *Phys. Rev. B* **80** 245320
[25] Danielson J R, Lee Y S, Prineas J P, Steiner J T, Kira M and Koch S W 2007 *Phys. Rev. Lett.* **99** 237401
[26] Jameson A D, Tomaino J L, Lee Y S, Prineas J P, Steiner J T, Kira M and Koch S W 2009 *Appl. Phys. Lett.* **95** 201107
[27] Dent C J, Murdin B N and Galbraith I 2003 *Phys. Rev. B* **67** 165312
[28] Zhang T Y and Zhao W 2008 *Chin. Phys. B* **17** 4285